



A Journal of the Gesellschaft Deutscher Chemiker

Angewandte Chemie

GDCh

International Edition

www.angewandte.org

Accepted Article

Title: Single-Atom Electrocatalysts from Multivariate MOFs for Highly Selective Reduction of CO₂ at Low Pressures

Authors: Hai-Long Jiang, Long Jiao, Weijie Yang, Gang Wan, Rui Zhang, Xusheng Zheng, Hua Zhou, and Shu-Hong Yu

This manuscript has been accepted after peer review and appears as an Accepted Article online prior to editing, proofing, and formal publication of the final Version of Record (VoR). This work is currently citable by using the Digital Object Identifier (DOI) given below. The VoR will be published online in Early View as soon as possible and may be different to this Accepted Article as a result of editing. Readers should obtain the VoR from the journal website shown below when it is published to ensure accuracy of information. The authors are responsible for the content of this Accepted Article.

To be cited as: *Angew. Chem. Int. Ed.* 10.1002/anie.202008787

Link to VoR: <https://doi.org/10.1002/anie.202008787>

Single-Atom Electrocatalysts from Multivariate MOFs for Highly Selective Reduction of CO₂ at Low Pressures

Long Jiao,^[a] Weijie Yang,^[b] Gang Wan,^[c] Rui Zhang,^[a] Xusheng Zheng,^[d] Hua Zhou,^[e] Shu-Hong Yu,^[a] and Hai-Long Jiang^{*[a]}

Dedication ((optional))

- [a] Dr. L. Jiao, R. Zhang, Prof. Dr. S.-H. Yu, Prof. Dr. H.-L. Jiang
Hefei National Laboratory for Physical Sciences at the Microscale, CAS Key Laboratory of Soft Matter Chemistry, Department of Chemistry, University of Science and Technology of China, Hefei, Anhui 230026, P. R. China
E-mail: jianglab@ustc.edu.cn
- [b] Dr. W. Yang
Department of Power Engineering, School of Energy, Power and Mechanical Engineering, North China Electric Power University, Baoding 071003, P.R. China
- [c] Dr. G. Wan
Materials Science Division, Argonne National Laboratory, Lemont, Illinois 60439, United States
- [d] Dr. X. Zheng
National Synchrotron Radiation Laboratory, University of Science and Technology of China, Hefei, Anhui 230029, P. R. China
- [e] Dr. H. Zhou
X-ray Science Division, Advanced Photon Source, Argonne National Laboratory, Lemont, Illinois 60439, United States

Supporting information for this article is given via a link at the end of the document.

Abstract: Single-atom catalysts (SACs) are of great interest due to their ultrahigh activity and selectivity. However, the lack of general synthetic protocol makes it difficult in the construction of model SACs to discern activity difference of diverse single-atom metal species. Herein, a universal synthetic strategy towards single-atom metal implanted N-doped carbon (M₁-N-C; M = Fe, Co, Ni and Cu) has been developed based on multivariate MOFs. The M₁-N-C catalysts, featuring identical parameters in chemical environment and support, provide an ideal platform to identify the differentiated activity of single-atom metal species. Upon being employed toward electrocatalytic CO₂ reduction, Ni₁-N-C exhibits a very high CO faradaic efficiency (FE) up to 96.8%, far surpassing Fe-, Co- and Cu-based M₁-N-C. Remarkably, the best-performed Ni₁-N-C even possesses excellent CO FE at low CO₂ pressures, which is more challenging, demonstrating a promising opportunity for the direct use of dilute CO₂ feedstock.

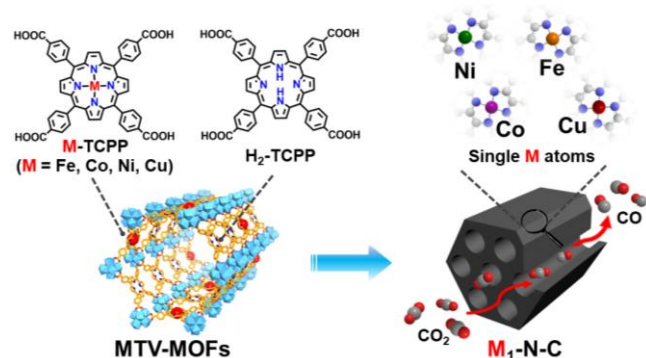
Introduction

Single-atom catalysts (SACs), as a new frontier of heterogeneous catalysis, have witnessed their great superiority in diverse reactions.^[1-9] With the active sites dispersed at atomic level, SACs possess ultrahigh catalytic activity and selectivity and facilitate the understanding of the structure-performance relationship at atomic/molecular scale.^[1-9] Generally, the catalytic performance of SACs is highly dependent on intrinsic properties of metal active sites and their surrounding microenvironment as well as physicochemical characteristics of supports, the latter of which pose great challenges to the nature identification of catalytic sites.^[10-12] Specifically, single-atom metal decorated N-doped carbon (M₁-N-C) materials, an important subclass of SACs, have been recognized as excellent electrocatalysts for CO₂ reduction reaction (CO₂RR).^[13-20] However, the carbon supports of the reported M₁-N-C materials always display various characteristics (pore structure, surface area, morphology,

etc.), making the activity of M₁-N-C tends to vary considerably even with the same metal center.^[21,22] On account of this, the general synthesis of M₁-N-C with a wide variety of metal species but similar microenvironment and supports is highly desired to identify the intrinsic activity of single-atom active sites.

Multivariate metal-organic frameworks (MTV-MOFs), an important subclass of MOFs incorporating multiple linkers of different functionalities within a single crystal, creating complexity within a skeleton in a controlled manner, have attracted growing attentions in many applications.^[23-26] The diversity of constituent units in MTV-MOFs create huge opportunities for the general construction of M₁-N-C with various metal centers. Meanwhile, it is ready for MTV-MOFs to control the variables of their derivatives, such as morphology, pore structure, surface area, elemental content, etc. Therefore, MTV-MOFs are ideal candidates to construct SACs and exclusively identify the intrinsic activities of different metal centers for CO₂RR. Meanwhile, the porous feature of MOFs can be largely inherited to their derivatives, which will benefit the exposure of active sites and thereby CO₂RR performance.^[27-29]

In addition to the active site identification, another critical issue in CO₂RR is the energy-consuming capture and purification process of CO₂. Specifically speaking, to achieve high selectivity, the currently reported CO₂RR are generally performed in pure CO₂.^[30-42] However, the actual concentration of CO₂ feedstock available from industrial processes such as coal power plant (5-15% CO₂) and steel/petrochemical industry (14-33% CO₂) is relatively low.^[43-45] Given the thermodynamic stability of the C=O bond (~ 806 kJ/mol) of CO₂ and its limited solubility in aqueous solution, low CO₂ concentration will significantly affect the activity, setting great barriers for the direct CO₂ utilization.^[45-47] Therefore, the development of efficient electrocatalysts for direct conversion of CO₂ at low pressures is extremely significant yet in its infancy and rarely achieved.^[43,45]



Scheme 1. Illustration showing the general fabrication of single-atom M_1 -N-C catalysts based on MTV-MOFs for electrocatalytic CO_2 reduction.

With all above in mind, a series of isostructural porphyrinic MTV-MOFs constructed by M-TCPP ($M = Fe, Co, Ni$ and Cu ; TCPP = tetrakis (4-carboxyphenyl)porphyrin) and H_2 -TCPP are selected as precursors. Thanks to the isomorphism of MTV-MOFs and spatial isolation of metal centers in M-TCPP, four kinds of M_1 -N-C ($M = Fe, Co, Ni$ and Cu) materials, featuring single metal atoms with very similar carbon support environment, have been obtained upon pyrolysis and serve as model catalysts to compare the intrinsic activity of diverse single-atom metal species (Scheme 1). Among all four M_1 -N-C ($M = Fe, Co, Ni$ and Cu) model catalysts for electrocatalytic CO_2 RR, Ni_1 -N-C exhibits the highest CO Faradic efficiency (FE) of 96.8% with a turnover frequency (TOF) up to $11315\ h^{-1}$ at $-0.8\ V$ in pure CO_2 . Theoretical calculations reveal that Ni_1 -N-C possesses the most positive value of the limiting potential difference between CO_2 reduction and H_2 evolution among all four M_1 -N-C catalysts, elucidating its high CO_2 RR selectivity in experiments. Remarkably, the best-performed Ni_1 -N-C catalyst is able to catalyze the reduction of diluted CO_2 , though a very challenging task, presenting excellent CO FE even at 30% and 15% CO_2 concentrations. This strongly proves the great superiority of Ni_1 -N-C toward selective CO_2 reduction under practical conditions.

Results and Discussion

Synthesis and characterization of M_1 -N-C.

A family of isostructural porphyrinic MTV-MOFs, named M-PCN-222 ($M = Fe, Co, Ni$ and Cu), have been successfully constructed by M-TCPP ($M = Fe, Co, Ni$ and Cu) and H_2 -TCPP via the mixed ligand strategy (Figure S1).^[28] With the general synthetic approach, the obtained M-PCN-222 involving different M-TCPP ligands present uniform rod-like shape with similar particle sizes, surface area and pore structure (Figure 1a, S2 and S3). Upon the pyrolysis of M-PCN-222 followed by ZrO_2 removal, M_1 -N-C ($M = Fe, Co, Ni$ and Cu) can be finally obtained. Taking Ni_1 -N-C as a representative, it shows a rod-like shape with a diameter of $\sim 200\ nm$, similar to those of Fe_1 -, Co_1 - and Cu_1 -N-C (Figure 1b and S4). In addition, no obvious metal nanoparticle is found in the TEM images of M_1 -N-C (Figure 1b and S4). N_2 adsorption measurements indicate that all M_1 -N-C possess similar surface area and pore size distribution (Figure S5, Table S2). Powder X-ray diffraction (XRD) patterns of all M_1 -

N-C present two broad peaks corresponding to the (002) and (101) planes of carbon and no peaks of metallic phase can be observed, in accordance with TEM results (Figure S6). In the Raman spectra of all M_1 -N-C catalysts, the intensity ratios of D band ($1345\ cm^{-1}$) and G band ($1590\ cm^{-1}$) are subject to small oscillation from 0.92 to 0.94, illustrating their similar graphitization degree (Figure S7, Table S2).

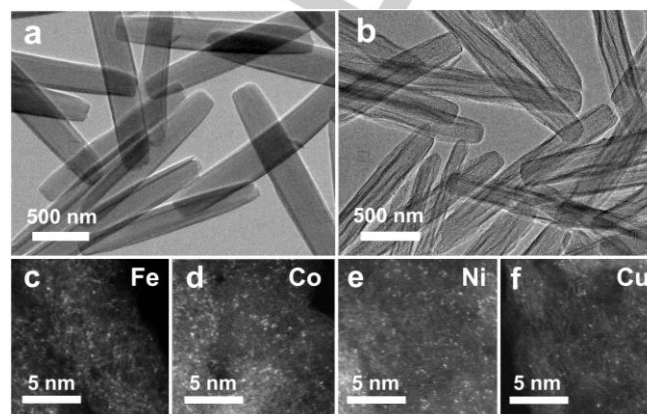


Figure 1. Transmission electron microscopy (TEM) images of (a) Ni -PCN-222 and (b) Ni_1 -N-C. The aberration-corrected HAADF-STEM images of (c) Fe_1 -N-C, (d) Co_1 -N-C, (e) Ni_1 -N-C and (f) Cu_1 -N-C.

X-ray photoelectron spectroscopy (XPS) was adopted to investigate the chemical compositions and electronic states of M_1 -N-C catalysts. The fitted N 1s XPS spectrum of Ni_1 -N-C clearly shows five characteristic peaks including pyridinic N ($398.7\ eV$), Ni-N moieties ($399.4\ eV$), pyrrolic N ($400.2\ eV$), graphitic N ($401.1\ eV$) and oxidized N ($402.6\ eV$) species (Figure S8a), confirming the existence of Ni-N bonding.^[28,48] The Ni 2p_{3/2} of Ni_1 -N-C presents a binding energy ($855.4\ eV$) located between Ni^0 ($853.0\ eV$) and Ni^{2+} ($855.7\ eV$), illustrating the partially oxidized Ni species originated from Ni-N species (Figure S9a).^[19,49] Moreover, the N K-edge near-edge X-ray absorption fine structure (NEXAFS) analysis has been further conducted. For the metal-free N-doped carbon (N-C) derived from PCN-222 involving H_2 -TCPP linker only, two π^* peaks corresponding to pyridinic N (peak a) and graphitic N (peak b), as well as a broaden peak (peak c) related to C-N σ^* bond, are detected (Figure S10a).^[50,51] In contrast, peak a broadens and splits into double peaks (a_1 and a_2) in Ni_1 -N-C, suggesting the existence of Ni atoms stabilized by pyridinic N (Figure 2a).^[51] Supportive results of XPS and N K-edge NEXAFS spectra are also obtained for Fe_1 -, Co_1 - and Cu_1 -N-C catalysts, all demonstrating the formation of corresponding M-N species (Figure S8, S9 and S10a). Quantitatively, the N content and Ni loading in Ni_1 -N-C are determined to be 4.94 and 1.75 wt%, similar to the other M_1 -N-C ($M = Fe, Co$ and Cu) catalysts (Table S2). In the aberration-corrected high-angle annular dark field scanning transmission electron microscope (HAADF-STEM) images, all M_1 -N-C catalysts are featured with bright dots randomly dispersed in the selected area, clearly presenting the full of atomically dispersed metal species in the domain of each M_1 -N-C (Figure 1c-f).

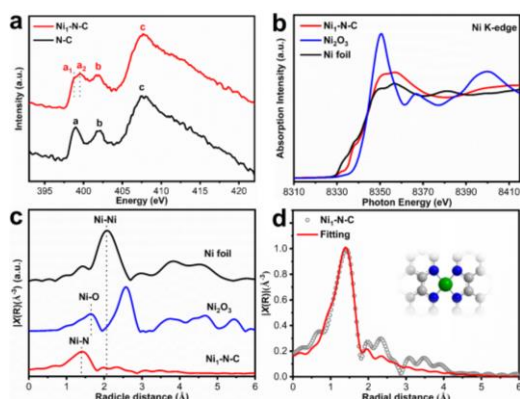


Figure 2. Structural characterizations. (a) Ni K-edge NEXAFS spectrum, (b) Ni K-edge XANES spectrum, (c) k^2 -weighted FT-EXAFS spectrum and (d) EXAFS fitting of Ni₁-N-C and optimized coordination environment of Ni atoms (inset).

Atomic structure analysis by X-ray absorption spectroscopy (XAS) studies.

To gain more information on the chemical environments of single metal atoms in M₁-N-C, X-ray absorption spectroscopy (XAS) was carried out. Taking Ni₁-N-C as an example, the adsorption edge of Ni₁-N-C in the Ni-K edge XANES spectra locates between Ni foil and Ni₂O₃, manifesting the positive charge state of Ni in Ni₁-N-C, in consistence with the XPS result (Figure 2b and S9a). In the Fourier transform-extended X-ray absorption fine structure (FT-EXAFS) spectrum of Ni₁-N-C, only one dominated peak at 1.4 Å associated to the Ni-N scattering path is presented and no Ni-Ni bond (~ 2.07 Å) can be observed, verifying the formation of single-atom Ni sites in Ni₁-N-C (Figure 2c). The EXAFS fitting suggests that the Ni is coordinated by four N atoms (Figure 2d, Table S3). The XAS analyses have been performed on Fe₁-, Co₁- and Cu₁-N-C as well and the results illustrate that all M₁-N-C possess similar metal coordination environment, featuring single-atom M coordinated by four N atoms (Figure S10 and S11, Table S3).

Electrocatalytic performance for CO₂RR in pure CO₂.

Encouraged by the above results, the M₁-N-C materials indeed feature almost identical structures except for different single metal atom sites. Therefore, they are ideal model catalysts to decode the intrinsic properties of these single-atom metals, by deducing their similar microenvironment and support factors, in electrochemical CO₂ reduction. As revealed by the linear sweep voltammetry (LSV) curves, Ni₁-N-C offers a much larger current response in pure CO₂ stream than the other M₁-N-C catalysts, indicating the significantly higher activity of Ni₁-N-C toward CO₂RR (Figure 3a and S12-S14). Furthermore, the Faradaic efficiencies (FEs) for M₁-N-C catalysts at different potentials have been investigated. The Ni₁-N-C shows the best CO selectivity with a highest CO FE of 96.8% at -0.8 V among all M₁-N-C catalysts (Figure 3b). Meanwhile, the high CO FE (over 90%) of Ni₁-N-C can be maintained in a wide potential range from -0.65 V to -0.95 V with H₂ as the only byproduct (no detectable liquid product), manifesting the excellent selectivity of Ni₁-N-C for CO₂RR (Figure 3b, S15 and S16). The Fe₁-N-C

catalyst is the second most active catalyst with a highest CO FE of 86.5%. In comparison, the remaining two catalysts, Co₁-N-C and Cu₁-N-C, display much lower CO FE caused by the very competitive HER process (Figure 3b and S15). Moreover, the TOF and CO partial current density (J_{CO}) of Ni₁-N-C reach 11315 h⁻¹ and 27 mA/cm² at -0.8 V, far surpassing those of the other three M₁-N-C catalysts (Figure 3c and S17). In fact, Ni₁-N-C shows a smaller Tafel slope (98 mV/decade) than that of Fe₁- (104 mV/decade), Co₁- (142 mV/decade) and Cu₁-N-C (118 mV/decade), indicating the more favorable kinetics of Ni₁-N-C. Meanwhile, Ni₁-N-C also shows smaller charge transfer resistance and larger electrochemical active surface area (ECSA) than other M₁-N-C catalysts, further supporting its much higher catalytic activity (Figure S18 and S19). In addition, the best performed Ni₁-N-C exhibits a long-term stability at -0.8 V for 10 h without obvious decay in current density and FE of CO (Figure 3e). The distinctly different performance of M₁-N-C model catalysts not only reveals that the catalytic activity and selectivity are strongly dependent on active metal species, but also unambiguously demonstrates that single-atom Ni site far exceeds the other metal sites in M₁-N-C. This conclusion is of significant yet being achieved previously, given the complexity of different SACs with different structural parameters such as metal loading, surface area, pore structure, coordination environment, etc. For better comparison, the metal-free N-C prepared from the PCN-222, with similar structural characteristics as M₁-N-C, has also been synthesized (Figure S1-S7, Table S1 and S2). It can be seen that N-C shows much lower current response, CO FE and turnover number (TON) and larger Tafel slope than Ni₁-N-C for CO₂ reduction, further supporting the importance role of single Ni atoms (Figure 3b, 3d, S20 and S21). Furthermore, Ni₁-N-C also shows better current response and CO FE than mix-Ni-N-C, the latter of which is derived from the mixture of Ni-TCPP and H₂-TCPP, further demonstrating the superiority of MOFs as precursors (Figure S22).

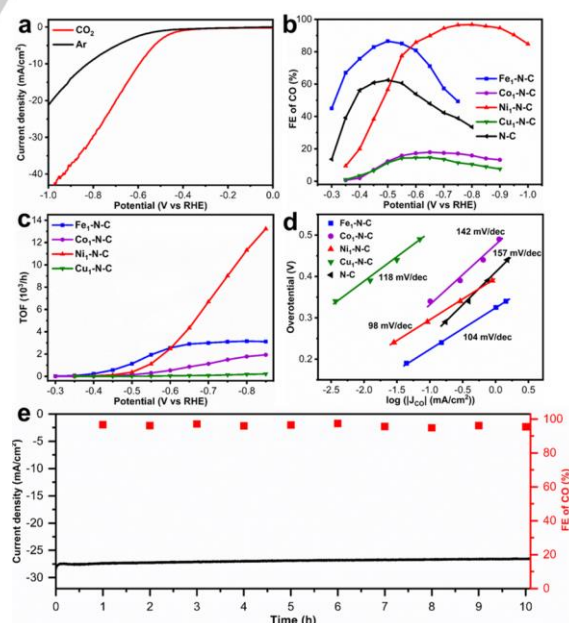


Figure 3. Electrochemical performances in pure CO₂. a) LSV curves of Ni₁-N-C in pure Ar- and CO₂-saturated 0.5 M KHCO₃. b) FEs and c) TOFs of M₁-N-C for CO₂RR in pure CO₂-saturated 0.5 M KHCO₃. d) Tafel plots of M₁-N-C for CO₂RR. e) Durability test of Ni₁-N-C at a constant potential of -0.8 V vs RHE in pure CO₂.

Theoretical Study of M₁-N-C for CO₂RR.

The above control experiments clearly demonstrate that all structural parameters in M₁-N-C catalysts are almost identical except for different metals. Therefore, M₁-N-C virtually provide ideal models for density functional theory (DFT) calculations to achieve reliable mechanism of diverse single-atom metal centers toward CO₂RR. Generally, the generation of CO by CO₂RR takes place in the following steps: (i) the CO₂ adsorption; (ii) the formation of *COOH; (iii) the formation of *CO and (iv) the CO desorption (* represents the adsorbed intermediates) (Figure 4a).^[40,52,53] Among the four elementary reaction steps, the formation of *COOH is calculated to be the rate-determining step (RDS) for all M₁-N-C catalysts (Figure 4b, S23 and S24). In all investigated M₁-N-C catalysts, Ni₁-N-C and Fe₁-N-C present much lower energy barriers for *COOH formation than Co₁-N-C and Cu₁-N-C, manifesting the much higher activity of Ni₁-N-C and Fe₁-N-C for CO₂ reduction (Figure 4b and S25). In addition, Ni₁-N-C also shows much lower energy barrier for CO desorption than Fe₁-N-C, illustrating the faster CO release from Ni₁-N-C (Figure 4b and S25). All above support the highest activity of Ni₁-N-C for CO₂ reduction. Given the existence of competitive HER process, the limiting potential difference between CO₂RR and HER ($U_L(\text{CO}_2) - U_L(\text{H}_2)$; $U_L = -\Delta G_0/e$) has been further calculated and employed as the descriptor of CO selectivity, where more positive value of $U_L(\text{CO}_2) - U_L(\text{H}_2)$ represents a higher CO₂RR selectivity than hydrogen evolution.^[35,54,55] As shown in Figure 4c, the $U_L(\text{CO}_2) - U_L(\text{H}_2)$ values for Fe₁-N-C, Co₁-N-C, Ni₁-N-C and Cu₁-N-C are -1.15, -1.98, -1.19 and -2.33 eV, respectively, which explains the CO selectivity following the order of Ni₁-N-C > Fe₁-N-C > Co₁-N-C > Cu₁-N-C, in high consistency with the experimental results (Figure 3b).

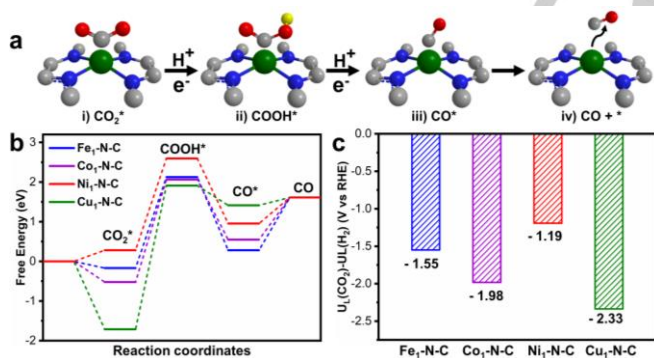


Figure 4. DFT calculations. a) Reaction paths and b) Free energy diagrams of CO₂ reduction to CO and c) The values of $U_L(\text{CO}_2) - U_L(\text{H}_2)$ for all M₁-N-C catalysts.

Electrocatalytic performance for the reduction of CO₂ at low pressures.

On the basis of the experimental evidences and theoretical calculations above, Ni₁-N-C incorporated with Ni-N₄ sites is highly efficient in selective CO₂ reduction. Inspired by this, the electrocatalytic performance of Ni₁-N-C toward low-concentration CO₂ reduction, which is a very challenging target in CO₂RR, has been further investigated. Prior to electrocatalytic measurements, the concentrations of protons ($[\text{H}^+]$) and

dissolved CO₂ ($[\text{CO}_2(\text{aq})]$) in aqueous solution under different CO₂ concentrations are calculated in detail based on dissociation equilibrium theories and Henry's law (Figure S26). Obviously, the $[\text{H}^+]$ and $[\text{CO}_2(\text{aq})]$ concentrations decrease significantly under lower CO₂ pressures, making CO₂ reduction more difficult according to the reaction equilibrium ($\text{CO}_2(\text{aq}) + 2\text{H}^+ + 2\text{e}^- \rightleftharpoons \text{CO} + \text{H}_2\text{O}$). Moreover, the equilibrium potentials are calculated based on the Nernst equation to be negatively shifted by 46 and 73 mV when CO₂ partial pressure decreased from 1 atm to 0.3 and 0.15 atm (Figure S27). The calculations conclude that the CO₂RR will be much more difficult at low CO₂ partial pressures from the viewpoint of thermodynamics. Therefore, this raises a higher demand for both activity and selectivity of the electrocatalysts, toward addressing this challenging goal.

In the experimental results, the LSV curves of Ni₁-N-C in CO₂/Ar mixed gas containing 30% and 15% CO₂ reasonably present higher current responses than that in pure Ar, indicating the evident CO₂ reduction activity under diluted CO₂ (Figure 5a). Using 30% CO₂ as the feed gas, the maximal CO FE of Ni₁-N-C reaches 91.6% with J_{CO} and TOF values of 6.69 mA/cm² and 1395 h⁻¹ at -0.8 V (Figure 5b and S28). Even though the concentration of CO₂ lowers to 15%, a high CO FE (83.2%) can still be observed at -0.75 V with J_{CO} and TOF of 2.91 mA/cm² and 607 h⁻¹ (Figure 5b and S28). It can be seen that even though the CO partial current density goes down with decreased CO₂ concentration, the CO FE still reaches above 80% under 15% CO₂ (Figure 5b and S29). In addition to the main product of CO, a small amount of H₂ as the only byproduct (no liquid product) can be detected at low CO₂ concentrations (Figure S30 and S16), similar to that in pure CO₂. Furthermore, Ni₁-N-C possesses stable current densities and CO FEs over 10 h at 30% and 15% CO₂ concentrations (Figure 5c). The results above clearly demonstrate the great potential of Ni₁-N-C for highly selective CO₂ reduction by using dilute CO₂ feedstock from industrial processes.

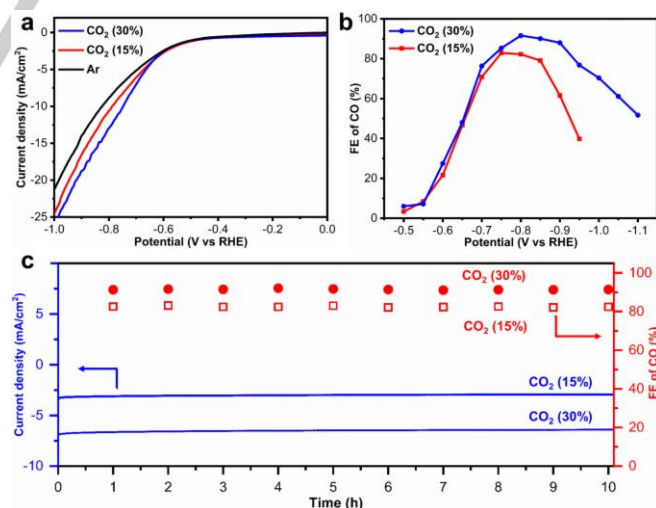


Figure 5. Electrochemical performances of CO₂ at low pressures. a) LSV curves and b) CO FE of Ni₁-N-C in 0.5 M KHCO₃ saturated with 30% and 15% CO₂. c) Durability tests of Ni₁-N-C at constant potential of -0.8 V under 30% CO₂ concentration and -0.75 V under 15% CO₂ concentration, respectively.

Conclusion

In summary, a series of single-atom catalysts (M_1 -N-C, $M = \text{Fe}$, Co , Ni and Cu), exhibiting almost identical pore structures and composition except for different single metal atoms, have been rationally constructed from isostructural porphyrinic MTV-MOFs. The obtained M_1 -N-C, featuring very similar microenvironment and support effect for metal active sites, are employed as ideal model catalysts to identify the intrinsic properties of single-atom metal species in electrochemical CO_2 reduction. Under pure CO_2 conditions, Ni_1 -N-C, with single-atom Ni as the active center, manifests the most satisfactory CO_2 RR performances with the highest CO selectivity up to 96.8%, followed by Fe_1 -N-C, then Co_1 -N-C and Cu_1 -N-C, among all investigated M_1 -N-C catalysts. DFT calculation results support the activity trend and illustrate that the best-performed Ni_1 -N-C, with the most positive value of $U_L(\text{CO}_2) - U_L(\text{H}_2)$, can efficiently promote CO_2 RR and suppress, to the maximum extent, the competitive HER. Given the ultrahigh selectivity of SACs, Ni_1 -N-C has also been employed to catalyze the reduction of CO_2 at low pressures, which is more challenging and rarely reported. Strikingly, the high selectivity of Ni_1 -N-C can be maintained even at 30% and 15% CO_2 concentrations, which are practical and directly available from industrial processes, further suggesting the superiority and ultrahigh selectivity of Ni_1 -N-C for CO_2 RR. This work provides a general route to a broad class of model SACs, which eliminate the interference of microenvironment and support effect, unambiguously unveiling the superior intrinsic performance of single Ni atoms to other Fe, Co and Cu counterparts in M_1 -N-C for CO_2 RR. Moreover, the preliminary results herein highlight the great potentials of Ni-based SACs for the direct electrocatalytic CO_2 conversion at low concentrations in future practical applications.

Acknowledgements

This work is supported by the NSFC (21725101, 21871244 and 21521001), China Postdoctoral Science Foundation (2019TQ0298, 2019M660151), International Partnership Program of CAS (211134KYSB20190109) and Fundamental Research Funds for the Central Universities (WK2060030029). Use of the Advanced Photon Source is supported by the U.S. Department of Energy, Office of Science, Office of Basic Energy Sciences, under Contract No. DE-AC02-06CH11357, and the Canadian Light Source and its funding partners. The calculations in this work are supported by the Supercomputing Center of University of Science and Technology of China.

Conflict of interest

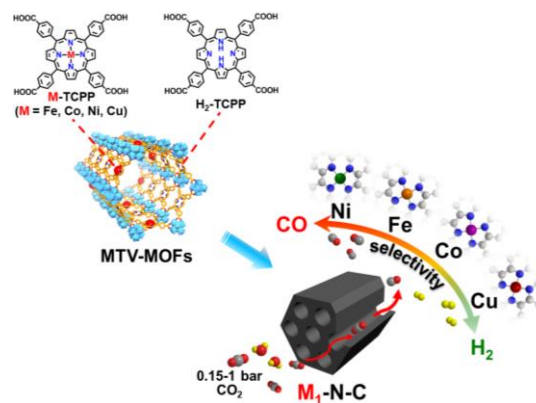
The authors declare no conflict of interest.

Keywords: Metal-organic frameworks • Single-atom catalysts • electrocatalysis • low pressure • CO_2 reduction

- [1] A. Wang, J. Li, T. Zhang, *Nat. Rev. Chem.* **2018**, *2*, 65-81.
- [2] J. Liu, *ACS Catal.* **2017**, *7*, 34-59.
- [3] S. Ji, Y. Chen, X. Wang, Z. Zhang, D. Wang, Y. Li, *Chem. Rev.* **2020**, DOI: 10.1021/acs.chemrev.9b00818.
- [4] C. Zhu, Q. Shi, S. Feng, D. Du, Y. Lin, *ACS Energy Lett.* **2018**, *3*, 1713-1721.
- [5] X. Li, X. Yang, Y. Huang, T. Zhang, B. Liu, *Adv. Mater.* **2019**, *31*, 1902031.
- [6] H. Zhang, G. Liu, Shi, L.; Ye, J. *Adv. Energy Mater.* **2018**, *8*, 1701343.
- [7] L. Zhang, Y. Jia, G. Gao, X. Yan, N. Chen, J. Chen, M. T. Soo, B. Wood, D. Yang, A. Du, X. Yao, *Chem*, **2018**, *4*, 285-297.
- [8] L. Jiao, H.-L. Jiang, *Chem* **2019**, *5*, 786-804.
- [9] C. Tang, Y. Jiao, B. Shi, J.-N. Liu, Z. Xie, X. Chen, Q. Zhang, S.-Z. Qiao, *Angew. Chem.* **2020**, *132*, 9256-9261; *Angew. Chem. Int. Ed.* **2020**, *59*, 9171-9176.
- [10] L. Zhao, Y. Zhang, L.-B. Huang, X.-Z. Liu, Q.-H. Zhang, C. He, Z.-Y. Wu, L.-J. Zhang, J. Wu, W. Yang, L. Gu, J.-S. Hu, L.-J. Wan, *Nat. Commun.* **2019**, *10*, 1278.
- [11] Y. Sun, L. Silvioli, N. R. Sahraie, W. Ju, J. Li, A. Zitolo, S. Li, A. Bagger, L. Arnarson, X. Wang, T. Moeller, D. Bernsmeier, J. Rossmeisl, F. Jaouen, P. Strasser, *J. Am. Chem. Soc.* **2019**, *141*, 12372-12381.
- [12] X. He, Q. He, Y. Deng, M. Peng, H. Chen, Y. Zhang, S. Yao, M. Zhang, D. Xiao, D. Ma, B. Ge, H. Ji, *Nat. Commun.* **2019**, *10*, 3663.
- [13] Y. Hou, Y.-B. Huang, Y.-L. Liang, G.-L. Chai, J.-D. Yi, T. Zhang, K.-T. Zang, J. Luo, R. Xu, H. Lin, S.-Y. Zhang, H.-M. Wang, R. Cao, *ACS Chem.* **2019**, *1*, 384-395.
- [14] Y. Cheng, S. Zhao, B. Johannessen, J. P. Veder, M. Saunders, M. R. Rowles, M. Cheng, C. Liu, M. F. Chisholm, R. D. Marco, H. M. Cheng, S. Z. Yang, S. P. Jiang, *Adv. Mater.* **2018**, *30*, 1706287.
- [15] T. Zheng, K. Jiang, N. Ta, Y. Hu, J. Zeng, J. Liu, H. Wang, *Joule* **2019**, *3*, 265-278.
- [16] X. Rong, H.-J. Wang, X.-L. Lu, R. Si, T.-B. Lu, *Angew. Chem.* **2020**, *132*, 1977-1981; *Angew. Chem. Int. Ed.* **2020**, *59*, 1961-1965.
- [17] J. Gu, C.-S. Hsu, L. Bai, H. M. Chen, X. Hu, *Science* **2019**, *364*, 1091-1094.
- [18] T. Wang, Q. Zhao, Y. Fu, C. Lei, B. Yang, Z. Li, L. Lei, G. Wu, Y. Hou, *Small Methods* **2019**, *3*, 1900210.
- [19] C. Yan, H. Li, Y. Ye, H. Wu, F. Cai, R. Si, J. Xiao, S. Miao, S. Xie, F. Yang, Y. Li, G. Wang, X. Bao, *Energy Environ. Sci.* **2018**, *11*, 1204-1210.
- [20] X.-L. Lu, X. Rong, C. Zhang, T.-B. Lu, *J. Mater. Chem. A* **2020**, *8*, 10695-10708.
- [21] H. Peng, F. Liu, X. Liu, S. Liao, C. You, X. Tian, H. Nan, F. Luo, H. Song, Z. Fu, P. Huang, *ACS Catal.* **2014**, *4*, 3797-3805.
- [22] J. Li, P. Pršija, T. Shinagawa, A. J. M. Fernández, F. Krumeich, K. Artyushkova, P. Atanassov, A. Zitolo, Y. Zhou, R. García-Muelas, N. López, J. Pérez-Ramírez, F. Jaouen, *ACS Catal.* **2019**, *9*, 10426-10439.
- [23] H. Deng, C. J. Doonan, H. Furukawa, R. B. Ferreira, J. Towne, C. B. Knobler, B. Wang, O. M. Yaghi, *Science* **2010**, *327*, 846-850.
- [24] A. Kirchon, L. Feng, H. F. Drake, E. A. Josepha, H.-C. Zhou, *Chem. Soc. Rev.* **2018**, *47*, 8611-8638.
- [25] X. Kong, H. Deng, F. Yan, J. Kim, J. A. Swisher, B. Smit, O. M. Yaghi, J. A. Reimer, *Science* **2013**, *341*, 882-885.
- [26] B. Li, H.-M. Wen, H. Wang, H. Wu, T. Yildirim, W. Zhou, B. Chen, *Energy Environ. Sci.* **2015**, *8*, 2504-2511.
- [27] S. Dang, Q.-L. Zhu, Q. Xu, *Nat. Rev. Mater.* **2017**, *3*, 17075.
- [28] L. Jiao, G. Wan, R. Zhang, H. Zhou, S.-H. Yu, H.-L. Jiang, *Angew. Chem.* **2018**, *130*, 8661-8665; *Angew. Chem. Int. Ed.* **2018**, *57*, 8525-8529.
- [29] K. J. Lee, J. H. Lee, S. Jeoung, H. R. Moon, *Acc. Chem. Res.* **2017**, *50*, 2684-2692.
- [30] J. Han, P. An, S. Liu, X. Zhang, D. Wang, Y. Yuan, J. Guo, X. Qiu, K. Hou, L. Shi, Y. Zhang, S. Zhao, C. Long, Z. Tang, *Angew. Chem.* **2019**, *131*, 12841-12846; *Angew. Chem. Int. Ed.* **2019**, *58*, 12711-12716.
- [31] H. Yang, Q. Lin, C. Zhang, X. Yu, Z. Cheng, G. Li, Q. Hu, X. Ren, Q. Zhang, J. Liu, C. He, *Nat. Commun.* **2020**, *11*, 593.
- [32] W. Luc, B. H. Ko, S. Kattel, S. Li, D. Su, J. G. Chen, F. Jiao, *J. Am. Chem. Soc.* **2019**, *141*, 9902-9909.
- [33] A. Guan, Z. Chen, Y. Quan, C. Peng, Z. Wang, T.-K. Sham, C. Yang, Y. Ji, L. Qian, X. Xu, G. Zheng, *ACS Energy Lett.* **2020**, *5*, 1044-1053.
- [34] J. Wu, Y. Huang, W. Ye, Y. Li, *Adv. Sci.* **2017**, *4*, 1700194.
- [35] W. Ren, X. Tan, W. Yang, C. Jia, S. Xu, K. Wang, S. C. Smith, C. Zhao, *Angew. Chem.* **2019**, *131*, 7046-7050; *Angew. Chem. Int. Ed.* **2019**, *58*, 6972-6976.

- [36] J. Li, Y. Kuang, Y. Meng, X. Tian, W.-H. Hung, X. Zhang, A. Li, M. Xu, W. Zhou, C.-S. Ku, C.-Y. Chiang, G. Zhu, J. Guo, X. Sun, H. Dai, *J. Am. Chem. Soc.* **2020**, *142*, 7276-7282.
- [37] X. Wei, Z. Yin, K. Lyu, Z. Li, J. Gong, G. Wang, L. Xiao, J. Lu, L. Zhuang, *ACS Catal.* **2020**, *10*, 4103-4111.
- [38] H. Zhong, M. Ghorbani-Asl, K. H. Ly, J. Zhang, J. Ge, M. Wang, Z. Liao, D. Makarov, E. Zschech, E. Brunner, I. M. Weidinger, J. Zhang, A. V. Krashennikov, S. Kaskel, R. Dong, X. Feng, *Nat. Commun.* **2020**, *11*, 1409.
- [39] M. A. Ghausi, J. Xie, Q. Li, X. Wang, R. Yang, M. Wu, Y. Wang, L. Dai, *Angew. Chem.* **2018**, *130*, 13319-13323; *Angew. Chem. Int. Ed.* **2018**, *57*, 13135-13139.
- [40] Q. Huang, Q. Li, J. Liu, Y.-R. Wang, R. Wang, L.-Z. Dong, Y.-H. Xia, J.-L. Wang, Y.-Q. Lan, *Matter* **2019**, *1*, 1656-1668.
- [41] A. Vasileff, X. Zhi, C. Xu, L. Ge, Y. Jiao, Y. Zheng, S.-Z. Qiao, *ACS Catal.* **2019**, *9*, 9411-9417.
- [42] A. Vasileff, Y. Zhu, X. Zhi, Y. Zhao, L. Ge, H. M. Chen, Y. Zheng, S.-Z. Qiao, *Angew. Chem.* **2020**, DOI: 10.1002/ange.202004846; *Angew. Chem. Int. Ed.* **2020**, DOI: 10.1002/anie.202004846.
- [43] X. Wang, A. Xu, F. Li, S.-F. Hung, D.-H. Nam, C. M. Gabardo, Z. Wang, Y. Xu, A. Ozden, A. S. Rasouli, A. H. Ip, D. Sinton, E. H. Sargent, *J. Am. Chem. Soc.* **2020**, *142*, 3525-3531.
- [44] G. V. Last, M. T. Schmick, *Environ. Earth. Sci.* **2015**, *74*, 1189-1198.
- [45] P. Hou, W. Song, X. Wang, Z. Hu, P. Kang, *Small* **2020**, *16*, 2001896.
- [46] T. Nakajima, Y. Tamaki, K. Ueno, E. Kato, T. Nishikawa, K. Ohkubo, Y. Yamazaki, T. Morimoto, O. Ishitani, *J. Am. Chem. Soc.* **2016**, *138*, 13818-13821.
- [47] Y. Wang, N.-Y. Huang, J.-Q. Shen, P.-Q. Liao, X.-M. Chen, J.-P. Zhang, *J. Am. Chem. Soc.* **2018**, *140*, 38-41.
- [48] Y.-N. Gong, L. Jiao, Y. Qian, C.-Y. Pan, L. Zheng, X. Cai, B. Liu, S.-H. Yu, H.-L. Jiang, *Angew. Chem.* **2020**, *132*, 2727-2731; *Angew. Chem. Int. Ed.* **2020**, *59*, 2705-2709.
- [49] C. Zhao, X. Dai, T. Yao, W. Chen, X. Wang, J. Wang, J. Yang, S. Wei, Y. Wu, Y. Li, *J. Am. Chem. Soc.* **2017**, *139*, 8078-8081.
- [50] L. Jiao, Y. Hu, H. Ju, C. Wang, M.-R. Gao, Q. Yang, J. Zhu, S.-H. Yu, H.-L. Jiang, *J. Mater. Chem. A* **2017**, *5*, 23170-23178.
- [51] P. Chen, T. Zhou, L. Xing, K. Xu, Y. Tong, H. Xie, L. Zhang, W. Yan, W. Chu, C. Wu, Y. Xie, *Angew. Chem.* **2017**, *129*, 625-629; *Angew. Chem. Int. Ed.* **2017**, *56*, 610-614.
- [52] Z. Zhang, J. Xiao, X.-J. Chen, S. Yu, L. Yu, R. Si, Y. Wang, S. Wang, X. Meng, Y. Wang, Z.-Q. Tian, D. Deng, *Angew. Chem.* **2018**, *130*, 16577-16580; *Angew. Chem. Int. Ed.* **2018**, *57*, 16339-16342.
- [53] P. Chen, Y. Jiao, Y.-H. Zhu, S.-M. Chen, L. Song, M. Jaroniec, Y. Zheng and S.-Z. Qiao, *J. Mater. Chem. A* **2019**, *7*, 7675-7682.
- [54] D. Kim, C. Xie, N. Becknell, Y. Yu, M. Karamad, K. Chan, E. J. Crumlin, J. K. Nørskov, P. Yang, *J. Am. Chem. Soc.* **2017**, *139*, 8329-8336.
- [55] C. Chen, X. Sun, X. Yan, Y. Wu, H. Liu, Q. Zhu, B. B. A. Bediako, B. Han, *Angew. Chem.* **2020**, *132*, 11216-11222; *Angew. Chem. Int. Ed.* **2020**, *59*, 11123-11129.

Entry for the Table of Contents



A series of single-atom metal implanted N-doped carbon (namely M₁-N-C; M = Fe, Co, Ni and Cu), with almost identical carbon support environment, are constructed based on multivariate MOFs. These M₁-N-C model catalysts make it possible to discern activity difference of diverse single-atom metal species toward CO₂ electroreduction. Significantly, the best-performed Ni₁-N-C is able to achieve highly selective reduction of CO₂ even at low pressures.